Journal of Nuclear Medicine, published on March 16, 2017 as doi:10.2967/jnumed.116.187807

Phase 2 study of 99mTc-trofolastat SPECT/CT to identify and localize prostate cancer in intermediate- and high-risk patients undergoing radical prostatectomy and extended pelvic lymph node dissection

Karolien E. Goffin (1), Steven Joniau (2), Peter Tenke (3), Kevin Slawin (4), Eric A. Klein (5), Nancy Stambler (6), Thomas Strack (6), John Babich (7), Thomas Armor (6), Vivien Wong (6)

(1) Nuclear medicine, UZ Leuven, Department of imaging and pathology, KU Leuven, Leuven, Belgium
(2) Urology, UZ Leuven, Department of Development and regeneration, KU Leuven, Leuven, Belgium
(3) Jahn Ferenc South Pest Hospital, Budapest, Hungary
(4) University of Texas Vanguard Urologic Institute, Houston, TX, USA
(5) Glickman Urological and Kidney Institute, Cleveland Clinic Foundation, Cleveland, OH, USA
(6) Progenics Pharmaceuticals, New York, NY, USA
(7) Weill Cornell Medicine, New York, NY, USA

Corresponding author and first author

Prof. dr. Karolien Goffin

Nuclear Medicine

University Hospital Leuven

Herestraat 49

3000 Leuven

Belgium

Telephone number: +3216343715

Fax number: +3216343759

E-mail address: Karolien.goffin@uzleuven.be

Word count: 4717

Financial support: Molecular Insight Pharmaceuticals, Inc. (a wholly-owned subsidiary of Progenics Pharmaceuticals), New York, NY, USA had a role in sponsoring the data and material in the study.

Running title: 99mTc-trofolastat SPECT/CT in PCa

ABSTRACT

Rationale: 99mTc-trofolastat (99mTc-MIP-1404), a small-molecule inhibitor of prostate-specific membrane antigen (PSMA), shows high potential to detect prostate cancer (PCa) non-invasively using single-photon-emission-computed-tomography (SPECT). We therefore wanted to assess the performance of 99mTc-trofolastat SPECT/CT in a phase 2 multi-center, multi-reader prospective study in patients with intermediate- and high-grade PCa, prior to radical prostatectomy and extended pelvic lymph node dissection, with histopathology as gold standard.

Methods: 105 PCa patients with an increased risk of lymph node involvement (LNI) received a pelvic 99mTc-trofolastat SPECT/CT prior to radical prostatectomy with extended pelvic lymph node dissection. Sensitivity of 99mTc-trofolastat for detection of PCa on a patient- and lobe-basis, using visual and semi-quantitative (tumor-to-background ratio, TBR) scores and of LNI was evaluated as well as correlation of uptake within the gland to Gleason scores (GS) and assessment of the predictive potential of 99mTc-trofolastat-uptake for LNI.

Results: PCa was detected in 98 patients (94%) with acceptable variability between readers. There was a significantly higher visual score and TBR in positive lobes compared to tumor-negative lobes. ROC analysis showed that visual scores more accurately discriminated lobes with GS ≤3+3 from ≥3+4, while TBRs discriminated high-grade disease from normal lobes better. Visual scores and TBRs correlated significantly with GS. 99mTc-trofolastat SPECT/CT detected LNI with sensitivity of 50%, and specificity of 87% and TBR values significantly predicted LNI with a sensitivity of 90%.

Conclusions: 99mTc-trofolastat SPECT/CT detects PCa with high sensitivity in patients with intermediate- and high-risk PCa compared to histology. It has potential to be used as surrogate marker for Gleason scores and predict LNI.

Keywords: 99mTc-trofolastat (99mTc-MIP-1404); SPECT/CT; prostate cancer; histopathology

INTRODUCTION

Imaging plays an increasingly important role in the initial diagnosis of PCa. Multiparametric magnetic resonance imaging (MRI) of the prostate is an emerging tool for accurate localization of the tumor within the prostate gland as well as for evaluating the extension of disease into neighboring tissues (*1*), but nuclear medicine techniques have also shown potential in the diagnosis and primary staging of PCa (*2*). One of the most recent developments within this field has been the development of radiotracers targeting PSMA, a trans-membrane 750 amino acid type II glycoprotein and zinc metalloenzyme which is primarily expressed in normal human prostate epithelium. PSMA is upregulated in PCa relocated from the cytosol to the cell membrane, thus becoming accessible to targeted binding by substrates or antibodies (*3,4*). Since PSMA is expressed by virtually all PCa and its expression is further increased in poorly differentiated, metastatic and hormone-refractory PCa, it is an attractive target for diagnosis and staging of this disease (*5-11*). Apart from radiotracers for imaging with positron emission tomography (PET), such as Gallium-68 (68Ga)-labelled Glu-urea-Lys(Ahx)-HBED-CC (68Ga-HBED-CC or 68Ga-PSMA-11) or 2-(3-(1-carboxy-5-[(6-[18F]fluoro-pyridine-3-carbonyl)-amino]-pentyl)-ureido)-pentanedioic acid (18F-DCFPyL) (*12-15*), small-molecule inhibitors of PSMA labeled with technetium-99m (99mTc) have been developed for imaging with SPECT (*16-18*), a nuclear medicine imaging technique that is more widely available than PET. Two variants of 99mTc-trofolastat, 99mTc-MIP-1404 and 99mTc-MIP-1405 were shown to have favorable biodistribution and kinetic behavior and visualized metastatic lesions in bone, prostate bed and lymph nodes in patients with metastatic PCa (*19*). Because prior work established that 99mTc-MIP-1404 had minimal activity in the bladder and had higher uptake in suspected lesions, this agent was chosen for use in the current study. To assess the performance characteristics of 99mTc-MIP-1404 (in the following 99mTc-trofolastat) imaging, we performed a phase 2 multi-center, multi-reader prospective study comparing imaging to histopathology as gold standard, in patients with intermediate- and high-grade primary PCa, subsequent to radical prostatectomy and extended pelvic lymph node dissection. Primary study objective was detection of disease at the gland level compared to histopathology. Secondary study objectives were evaluation of the location and the extent of disease within the prostate gland and the prediction of lymph node status based on imaging.

MATERIALS AND METHODS

Patients

From September 2012 to October 2013, 105 patients with histologically proven adenocarcinoma of the prostate gland and at high-risk for LN metastases by a stage of cT3, cT4, or a total nomogram score of ≥ 130 (*20*), who were scheduled to undergo radical prostatectomy with extended pelvic lymph node dissection, were prospectively included in this multicenter study. A complete medical history including tumor grade, clinical stage and prostate specific antigen, any past/present PCa therapies and demographic information was collected. The local ethics committees approved the study and written informed consent was obtained from all patients before inclusion (NCT01667536). Baseline characteristics of the study population can be found in Table 1.

Pelvic MRI

At least one day prior to study drug administration, patients underwent contrast enhanced MRI of the pelvis (T1- and T2-weighted images with at least a 1.5 Tesla magnet utilizing a torso phased-array coil or combined endorectal-body phased-array coil). Sequences included axial and coronal pre- and post-contrast FAT-SAT protocols with a slice thickness of ≤5 mm.

99mTc-trofolastat imaging

In this study, an optimized and simplified method was used to radiolabel the drug precursor with 99mTc, compared to the labeling procedure that has been described earlier (*19*). Three to 6 hours prior to imaging, an activity of 740±111 MBq 99mTc-trofolastat was injected intravenously. Simultaneous anterior and posterior whole-body scans were obtained using a scan speed of 10 cm/min. This was followed by a pelvic dual-head SPECT/CT (step-and-shoot, 30 sec per stop, 60-64 projections per head; CT 130 kVp, 10-30 mAs). SPECT acquisitions were iteratively reconstructed on a commercially available workstation (Segami; Columbia, MD, USA) using ordered subset expectation maximization, applying scatter correction and CT-based attenuation correction at ICON Medical Imaging (Warrington, PA, USA).

Surgery

Patients underwent a standard of care radical prostatectomy with a standardized extended pelvic lymph node dissection including obturator and iliac regions, at least 1 week, but no more than 3 weeks after 99mTc-trofolastat imaging. Surgical staff was blinded to the results of 99mTc-trofolastat imaging and labeled all specimens to correlate to the specific anatomical location of removal.

Surgical pathology

Immediately following surgery, specimens were prepared for local histopathological processing and analysis using a study-specific pathology manual. Briefly, gross handling of the prostate gland and lymphadenectomy specimens included whole mount assessment and sectioning of the prostate gland, overall measurement of specimen size, palpation to identify lymph nodes in fatty tissue, dissection and description of identified lymph nodes and submission of lymph nodes in their entirety plus all remaining fibroadipose tissue for each harvested regional packet.

Image analysis

99mTc-trofolastat images were evaluated centrally and independently by three board-certified nuclear medicine physicians, blinded to clinical information. Each reviewer received a brief training session, which included review of 10-20 normal and abnormal cases from previous clinical trials.

For visual evaluation of 99mTc-trofolastat-uptake within the prostate gland, a binary evaluation of the presence or absence of increased uptake was made. For semi-quantitative evaluation of 99mTc-trofolastat-uptake, the TBR was calculated for each visually detected lesion or other tissue within each lobe (right/left) of the prostate using the quotient of maximal counts within a circular region-of-interest and mean counts within the obturator muscle (Supplemental Fig. 1). Furthermore, a detailed visual scoring scale was used to score uptake in each lobe (right/left) with higher scores representing more intense levels of uptake, as judged by the TBR (Supplemental Table 1). For LN assessment, abnormal LN uptake was defined as abnormal distribution of activity in tissues and organs greater than local background and consistent with sites of PCa metastatic spread and consensus between readers was defined as the agreement of the at least two of readers for each case.

Contrast enhanced T1- and T2-weighted MR images of the pelvis and available functional sequences were evaluated centrally by an experienced radiologist blinded to clinical information. Each patient with evaluable images was assessed for the presence or absence of PCa at the level of the whole prostate gland, right and left lobes of the prostate gland and pelvic lymph nodes.

Statistical analysis

The primary analysis estimated the ability of 99mTc-trofolastat to detect histologically confirmed PCa in the prostate and was based on the calculation of the percentage of positive 99mTc-trofolastat scans of the whole prostate, using histopathology results as gold standard. The true-positive fraction (equivalent to sensitivity) was calculated. Secondary efficacy parameters involved the calculation of the false-positive fraction (equivalent to 1-specificity) of 99mTc-trofolastat compared to histopathology within the prostate gland (lobe-level). Spearman's correlation coefficient was used to assess associations between TBR and visual scores and post-prostatectomy GS. Student's t-tests were performed between mean values of TBR of positive and negative findings, GS, and prior treatment across each independent reader and the average of three readers. Median visual scores were tested using a Wilcoxon rank-sum test. For all analyses, a p-value <0.05 was considered significant. Receiver operating characteristic (ROC) analyses and areas under the curve (AUCs) with corresponding 95% confidence intervals were calculated for TBR and reader scores using positive and negative controls of any PCa, GS >3+4 and LNI and optimal cut-off values determined by Youden's J statistic. Statistical analysis was performed using R version 3.2.1 (R Foundation for Statistical Computing, Vienna, Austria). Spearman's correlation and the Wilcoxon rank-sum test were calculated using JMP version 11.2.0 (SAS Institute Inc., Cary, USA).

RESULTS

Detection of PCa within the prostate gland

From the 105 patients of the study population, SPECT/CT images of 104 patients were available for evaluation. One patient did not undergo SPECT/CT imaging, one other patient only had SPECT imaging and was excluded for semi-quantitative analysis and six patients did not have an evaluable MRI.

On a patient basis, PCa was detected by a consensus of at least two of the three readers in 98 of 104 patients (94%) using 99mTc-trofolastat SPECT/CT and confirmed by histopathologic findings. There was an acceptable variability in true-positive fraction between readers: 89%, 85% and 98%, respectively. MRI and 99mTc-trofolastat SPECT/CT results could be compared in 98 patients. In this subgroup, detection rates were 94% and 86% for SPECT/CT and MRI, respectively. Since all patients were confirmed by pathologic evaluation to have adenocarcinoma of the prostate gland, false-positive fraction could not be calculated on a patient basis. Representative examples of a positive 99mTc-trofolastat SPECT/CTs can be seen in Fig. 1.

Of 206 evaluable prostate lobes, 24 were normal by histopathology (13 right, 11 left) and were used as controls in further analyses. Compared to control lobes, there was a significantly higher median visual score in positive lobes 3.0 vs 0, $p < 0.0001$) (Fig. 2; Supplemental Table 2). Semi-quantitative analysis showed significantly higher average TBRs in PCa positive lobes compared to control lobes (26.1 vs 13.5, $p < 0.0015$) (Fig. 2).

ROC analysis of the median visual scores showed a similar AUC of 0.74 for discrimination of any PCa per lobe and 0.72 for areas of the gland containing GS ≥3+4 disease (Fig. 3) with optimal cut-off values of 2.5 and 3.5, respectively. Conversely, ROC analysis of semi-quantitative TBRs showed AUCs between 0.70 and 0.78, with a lower AUC value for detection of any grade PCa compared with areas of the gland containing GS ≥3+4 disease (Fig. 3) and optimal cut-off values of 12 and 20, respectively.

Correlation of 99mTc-trofolastat uptake to Gleason scores

Median visual scores were significantly higher in PCa positive lobes with GS ≥3+4 compared to ≤3+3 (4.0 vs 1.0, $p < 0.0001$), as were TBRs (30.8 vs 13.1, $p < 0.0001$) (Figs.1 and 2). Moreover, the average visual score correlated significantly with GS (Spearman's $\rho = 0.48$, $p < 0.0001$), as did TBRs (Spearman's $\rho = 0.53$, $p < 0.0001$) (Fig. 4).

Lymph Node Assessment

A total of 3025 nodes were removed from 103 patients (mean 29.6, range 1-88). Of these, 79 nodes were positive by pathology in 33 patients (32%). A representative example of accurately detected

LNI can be seen in Supplemental Fig. 2. At the patient level, sensitivity and specificity for detection of lymph node invasion were 33.3% and 88.4%, respectively. When patients that were currently being treated with androgen deprivation therapy (ADT) were excluded, sensitivity and specificity increased to 50.0% and 87.3%, respectively. On MRI, sensitivity and specificity for detection of lymph node invasion were 12.5% and 95.5% in all patients, and 15.8% and 96.2% when patients that were receiving ADT were excluded.

TBR values of the prostatic lesion were found to be a predictor of LNI in evaluable treatment-naïve patients. ROC analysis showed an overall diagnostic accuracy of 77% (AUC 0.77 95% CI 0.65-0.89) with a cutoff of 30.2 (Fig. 5). This yielded a sensitivity of 90% (18/20) and specificity of 67% (37/55) for the presence of LNI following a standardized extended pelvic lymph node dissection.

DISCUSSION

In this multi-center prospective phase 2 study, we demonstrate that 99mTc-trofolastat (99mTc-MIP1404) SPECT/CT imaging is able to detect varying degrees of primary PCa with high accuracy, confirmed by postoperative histopathology of the primary tumor and lymph nodes. Increased uptake within the tumoral lesion was detected in 94% of patients, compared to 86% considered abnormal on MRI. However, mainly standard anatomical T1- and T2-weighted MR sequences were used in this study to evaluate the whole pelvis, which may explain the lower detection rate of MRI in primary lesions. Eiber and colleagues found that ^{68}Ga-PSMA PET (detection rate 92%) outperformed multiparametric MRI (detection rate 66%) to detect primary PCa in 53 eligible patients. Combined 68Ga-PSMA PET/MRI showed even higher the best detection rate (98%) (*21*). Giesel et al. found good allocation of PCa in accordance to biopsy with multiparametric MRI as well as ^{68}Ga-PSMA PET/CT in 10 patients with primary PCa with visually concordant tumor extension on ^{68}Ga-PSMA PET/CT using an isocontour 50% of SUV_{max} compared to multiparametric MRI (*22*). Contrasting results were described by Rowe et al., who found a higher sensitivity for MRI than for 18F-DCFBC PET in detecting primary PCa of variable GS (6 to 9) in a segment-based analysis in 13 patients. Specificity on the other hand was higher for 18F-DCFBC PET, especially for high-grade lesions with a volume larger than 1.0 ml (*23*).

Image interpretation of 99mTc-trofolastat SPECT/CT images was performed by 3 readers with no prior experience with 99mTc-trofolastat and was proven to be easy and reliable, since detection rates and visual scores had acceptable variability. Visual reader scores as well as semi-quantitative TBRs were significantly higher in PCa positive lobes compared to normal lobes. ROC analysis demonstrated that quantitative scoring in the form of TBR may be better for discriminating higher-grade PCa from normal prostate tissue, while semi-quantitative visual scoring appeared to better differentiate normal tissue and low-grade PCa with a GS ≤ 3+3 from higher-grade PCa with a GS ≥ 3+4. This finding suggests that readers used other visual information such as the pattern of uptake as an additional cue in borderline cases with lower TBR values.

In line with previous findings where higher PSMA expression was seen with increasing tumor aggressiveness (*24*), 99mTc-trofolastat-uptake in prostate lesions was correlated to GS with higher visual reader scores and higher TBRs at higher GS. Using PMSA PET-imaging, contrasting results have been described with a significant correlation between GS and tracer uptake in a number of studies (*23,25,26*) and no significant correlation in others (*21,27*). Similarly, it has been shown that both apparent diffusion coefficient and MR spectroscopy are correlated with Gleason grade (*28-30*). Thus, there is a potential role for 99mTc-trofolastat imaging not only in localizing tumor but also in identifying areas of more aggressive tumor that could be targeted by transrectal ultrasound- or MRI-guided prostate biopsy or to guide repeat prostate biopsy in patients with previous negative biopsies, thus improving medical decisions.

At present, lymph node dissection is still the only reliable staging tool for LNI in high-risk PCa, since nomograms lack accuracy. On a patient level, 99mTc-trofolastat imaging shows a low sensitivity, but good specificity at detecting LNI. These findings are in line with previous studies. Budaüs et al. report a sensitivity of 33% as well using 68Ga-PSMA PET/CT (*31*). Maurer et al. demonstrated that 68Ga-PSMA PET/CT was significantly better in detecting metastatic lymph nodes compared to conventional imaging (CT or MRI) in 130 patients with primary intermediate or high grade PCa. 31% of patients presented with lymph node metastases at histology and 68Ga-PSMA PET/CT had a patient-based sensitivity of 66%, specificity of 99% and accuracy of 88%. In a LN field based analysis (16% of 117 LN field positive at histology) sensitivity, specificity and accuracy of 68Ga-PSMA PET/CT were 68%, 99% and 95%, respectively (*32*). When excluding patients that were being treated with ADT in our study population,

sensitivity increased to 50%. ADT may therefore be seen as a negative factor for visualizing of LNI. This finding appears to contradict findings of 68Ga-PSMA PET/CT seven days following initiation of ADT may increase PSMA expression and improve detection rates by PSMA imaging (*33*). However, long-standing ADT treatment also reduces tumor mass and thus, the ability for PSMA imaging ligands to visualize now much smaller lesions. Thus, we believe this explains the reduced diagnostic performance of 99mTc-trofolastat SPECT/CT in our patients who had been on ADT for much longer times than 7 days prior to SPECT imaging. Furthermore, we show that 99mTc-trofolastat-uptake in the prostate lesion itself is a predictor of LNI, with a good sensitivity of 90%, but a somewhat lower specificity of 67% using a TBR of 30.2.

In the current study, only a small number of patients with low GS were present. It will therefore be important to study the performance of 99mTc-trofolastat SPECT/CT in a larger cohort of patients with low-risk PCa, especially since it may be a useful tool for active surveillance in these patients, ultimately determining which patients have to be moved to active treatment when uptake in the lesion increases, representing a higher GS or progressing lesion. Likewise, only patients with primary PCa were included in this study. Recent data have shown, however, the large potential of PSMA-targeted imaging in restaging patients with biochemical recurrence after initial curative treatment (*13,34*), using gallium-68 labelled compounds and PET-imaging. PET/CT cameras are however not widely available in general hospitals and the cost of a gallium-68 generator is high, demonstrating the remaining need for an easily produced 99m-technetium labelled PSMA agent that can be imaged using SPECT. The usefulness of 99mTc-trofolastat imaging of biochemical recurrence however still needs to be proven, but shows potential in this setting. Similarly, 99mTc-trofolastat SPECT/CT can also be used as a baseline staging tool in patients with disseminated disease that are candidates for PSMA-based radionuclide treatment such as 131I-MIP 1095 (*35*) or 177Lu-labelled compounds (*36*).

CONCLUSION

99mTc-trofolastat SPECT/CT imaging is able to detect primary PCa with high accuracy, as demonstrated in this multi-center Phase 2 study. Its uptake within the prostate lesion is correlated to Gleason scores and may predict lymph node involvement in patients with intermediate- and high-risk PCa

compared to histology. Further studies in other patient populations are warranted to evaluate the broader applicability of this promising PSMA-based imaging agent.

FINANCIAL DISCLOSURE

Molecular Insight Pharmaceuticals, Inc. (a wholly-owned subsidiary of Progenics Pharmaceuticals), Tarrytown, NY, USA had a role in sponsoring the data and material in the study. T. Armor, N. Stambler, V. Wong, T. Strack are full-time employees of Progenics Pharmaceuticals. N. Stambler and V. Wong are shareholders of Progenics Pharmaceuticals, Inc.

ACKNOWLEDGEMENTS

We thank W. Ellis, B. Alekseev, I. Buzogány, S. Mishugin, J. Stolz, V. Student, V. Matveev, R.J. Karnes, D. Sherr, B. Yuh, T. Keane, D. Jarrard, E.J. Trabulsi, A. Briganti, O. Karyakin and M. Hora for their help in acquiring the 99mTc-trofolastat SPECT/CT Imaging and performing surgery.

REFERENCES

1. Murphy G, Haider M, Ghai S, Sreeharsha B. The expanding role of MRI in prostate cancer. *AJR Am J Roentgenol.* 2013;201:1229-1238.

2. Mapelli P, Picchio M. Initial prostate cancer diagnosis and disease staging--the role of choline-PET-CT. *Nat Rev Urol.* 2015;12:510-518.

3. Kratochwil C, Giesel FL, Eder M, et al. [(177)Lu]Lutetium-labelled PSMA ligand-induced remission in a patient with metastatic prostate cancer. *Eur J Nucl Med Mol Imaging.* 2015;42:987-988.

4. Smith-Jones PM, Vallabahajosula S, Goldsmith SJ, et al. In vitro characterization of radiolabeled monoclonal antibodies specific for the extracellular domain of prostate-specific membrane antigen. *Cancer Res.* 2000;60:5237-5243.

5. Kinoshita Y, Kuratsukuri K, Landas S, et al. Expression of prostate-specific membrane antigen in normal and malignant human tissues. *World J Surg.* 2006;30:628-636.

6. Murphy GP, Elgamal AA, Su SL, Bostwick DG, Holmes EH. Current evaluation of the tissue localization and diagnostic utility of prostate specific membrane antigen. *Cancer.* 1998;83:2259-2269.

7. Ghosh A, Heston WD. Tumor target prostate specific membrane antigen (PSMA) and its regulation in prostate cancer. *J Cell Biochem.* 2004;91:528-539.

8. Henry MD, Wen S, Silva MD, Chandra S, Milton M, Worland PJ. A prostate-specific membrane antigen-targeted monoclonal antibody-chemotherapeutic conjugate designed for the treatment of prostate cancer. *Cancer Res.* 2004;64:7995-8001.

9. Elsasser-Beile U, Buhler P, Wolf P. Targeted therapies for prostate cancer against the prostate specific membrane antigen. *Curr Drug Targets.* 2009;10:118-125.

10. Elsasser-Beile U, Reischl G, Wiehr S, et al. PET imaging of prostate cancer xenografts with a highly specific antibody against the prostate-specific membrane antigen. *J Nucl Med.* 2009;50:606-611.

11. Milowsky MI, Nanus DM, Kostakoglu L, Vallabhajosula S, Goldsmith SJ, Bander NH. Phase I trial of yttrium-90-labeled anti-prostate-specific membrane antigen monoclonal antibody J591 for androgen-independent prostate cancer. *J Clin Oncol.* 2004;22:2522-2531.

12. Eder M, Schafer M, Bauder-Wust U, et al. 68Ga-complex lipophilicity and the targeting property of a urea-based PSMA inhibitor for PET imaging. *Bioconjug Chem.* 2012;23:688-697.

13. Afshar-Oromieh A, Avtzi E, Giesel FL, et al. The diagnostic value of PET/CT imaging with the (68)Ga-labelled PSMA ligand HBED-CC in the diagnosis of recurrent prostate cancer. *Eur J Nucl Med Mol Imaging.* 2015;42:197-209.

14. Eiber M, Maurer T, Souvatzoglou M, et al. Evaluation of Hybrid 68Ga-PSMA Ligand PET/CT in 248 Patients with Biochemical Recurrence After Radical Prostatectomy. *J Nucl Med.* 2015;56:668-674.

15. Szabo Z, Mena E, Rowe SP, et al. Initial Evaluation of [(18)F]DCFPyL for Prostate-Specific Membrane Antigen (PSMA)-Targeted PET Imaging of Prostate Cancer. *Mol Imaging Biol.* 2015;17:565-574.

16. Hillier SM, Maresca KP, Lu G, et al. 99mTc-labeled small-molecule inhibitors of prostate-specific membrane antigen for molecular imaging of prostate cancer. *J Nucl Med.* 2013;54:1369-1376.

17. Barrett JA, Coleman RE, Goldsmith SJ, et al. First-in-man evaluation of 2 high-affinity PSMA-avid small molecules for imaging prostate cancer. *J Nucl Med.* 2013;54:380-387.

18. Robu S, Schottelius M, Eiber M, et al. Preclinical evaluation and first patient application of 99mTc-PSMA-I&S for SPECT imaging and radioguided surgery in prostate cancer. *J Nucl Med.* 2017;58:235-242.

19. Vallabhajosula S, Nikolopoulou A, Babich JW, et al. 99mTc-labeled small-molecule inhibitors of prostate-specific membrane antigen: pharmacokinetics and biodistribution studies in healthy subjects and patients with metastatic prostate cancer. *J Nucl Med.* 2014;55:1791-1798.

20. Godoy G, Chong KT, Cronin A, et al. Extent of pelvic lymph node dissection and the impact of standard template dissection on nomogram prediction of lymph node involvement. *Eur Urol.* 2011;60:195-201.

21. Eiber M, Weirich G, Holzapfel K, et al. Simultaneous Ga-PSMA HBED-CC PET/MRI Improves the Localization of Primary Prostate Cancer. *Eur Urol.* 2016;70:829-836.

22. Giesel FL, Sterzing F, Schlemmer HP, et al. Intra-individual comparison of Ga-PSMA-11-PET/CT and multi-parametric MR for imaging of primary prostate cancer. *Eur J Nucl Med Mol Imaging.* 2016;43:1400-1406.

23. Rowe SP, Gage KL, Faraj SF, et al. (1)(8)F-DCFBC PET/CT for PSMA-Based Detection and Characterization of Primary Prostate Cancer. *J Nucl Med.* 2015;56:1003-1010.

24. Perner S, Hofer MD, Kim R, et al. Prostate-specific membrane antigen expression as a predictor of prostate cancer progression. *Hum Pathol.* 2007;38:696-701.

25. Rahbar K, Weckesser M, Huss S, et al. Correlation of Intraprostatic Tumor Extent with 68Ga-PSMA Distribution in Patients with Prostate Cancer. *J Nucl Med.* 2016;57:563-567.

26. Uprimny C, Kroiss AS, Decristoforo C, et al. 68Ga-PSMA-11 PET/CT in primary staging of prostate cancer: PSA and Gleason score predict the intensity of tracer accumulation in the primary tumour. *Eur J Nucl Med Mol Imaging.* 2017. doi: 10.1007/s00259-017-3631-6.

27. Zamboglou C, Wieser G, Hennies S, et al. MRI versus (68)Ga-PSMA PET/CT for gross tumour volume delineation in radiation treatment planning of primary prostate cancer. *Eur J Nucl Med Mol Imaging.* 2016;43:889-897.

28. Barentsz JO, Richenberg J, Clements R, et al. ESUR prostate MR guidelines 2012. *Eur Radiol.* 2012;22:746-757.

29. Claus FG, Hricak H, Hattery RR. Pretreatment evaluation of prostate cancer: role of MR imaging and 1H MR spectroscopy. *Radiographics.* 2004;24 Suppl 1:S167-180.

30. Choi YJ, Kim JK, Kim N, Kim KW, Choi EK, Cho KS. Functional MR imaging of prostate cancer. *Radiographics.* 2007;27:63-75.

31. Budaus L, Leyh-Bannurah SR, Salomon G, et al. Initial Experience of (68)Ga-PSMA PET/CT Imaging in High-risk Prostate Cancer Patients Prior to Radical Prostatectomy. *Eur Urol.* 2016;69:393-396.

32. Maurer T, Gschwend JE, Rauscher I, et al. Diagnostic Efficacy of (68)Gallium-PSMA Positron Emission Tomography Compared to Conventional Imaging for Lymph Node Staging of 130 Consecutive Patients with Intermediate to High Risk Prostate Cancer. *J Urol.* 2016;195:1436-1443.

33. Hope TA, Truillet CC, Ehman EC, et al. Imaging Response to Androgen Receptor Inhibition Using 68Ga-PSMA-11 PET: First Human Experience. *J Nucl Med.* 2017;58:81-84.

34. Eiber M, Nekolla SG, Maurer T, Weirich G, Wester HJ, Schwaiger M. (68)Ga-PSMA PET/MR with multimodality image analysis for primary prostate cancer. *Abdom Imaging.* 2015;40:1769-1771.

35. Zechmann CM, Afshar-Oromieh A, Armor T, et al. Radiation dosimetry and first therapy results with a (124)I/ (131)I-labeled small molecule (MIP-1095) targeting PSMA for prostate cancer therapy. *Eur J Nucl Med Mol Imaging.* 2014;41:1280-1292.

36. Ahmadzadehfar H, Rahbar K, Kurpig S, et al. Early side effects and first results of radioligand therapy with (177)Lu-DKFZ-617 PSMA of castrate-resistant metastatic prostate cancer: a two-centre study. *EJNMMI Res.* 2015;5:36-43.

FIGURES WITH LEGENDS

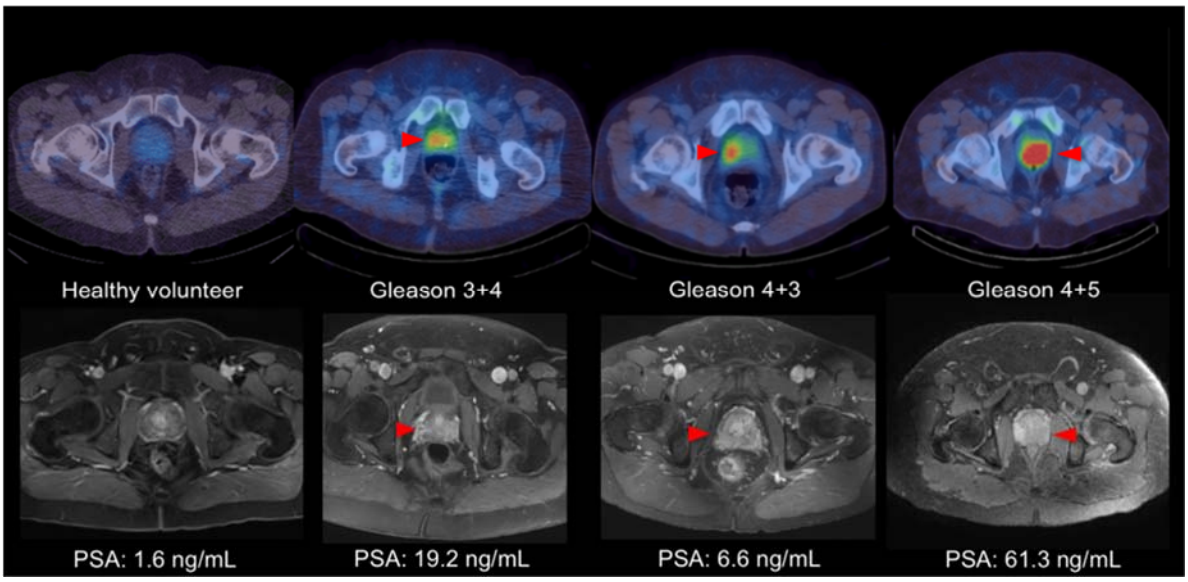

FIGURE 1: Examples of fused axial 99mTc-trofolastat SPECT/CT reconstructions from a previously acquired healthy volunteer (first column) and three study patients (top row), and matching axial contrast enhanced T1-weighted MRIs (bottom row) arranged by GS from left to right. Red arrow heads indicate location of histologically confirmed primary prostate lesions.

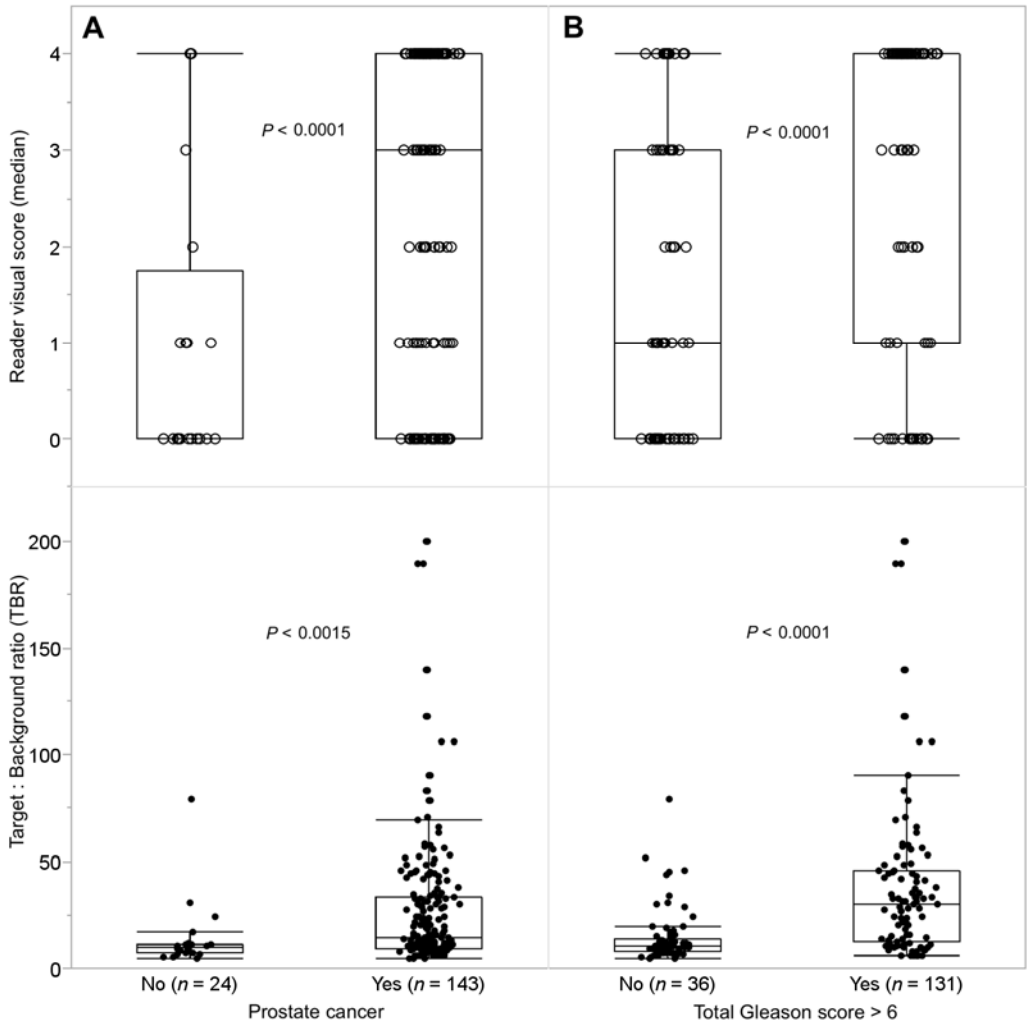

FIGURE 2. Box-and-whisker plots of mean reader scores (top row, open circles) and TBR values (bottom row, solid circles) in prostate lobes: (A) without PCa and with PCa; (B) with GS ≤6 and GS ≥7. Box and whiskers represent mean and interquartile range.

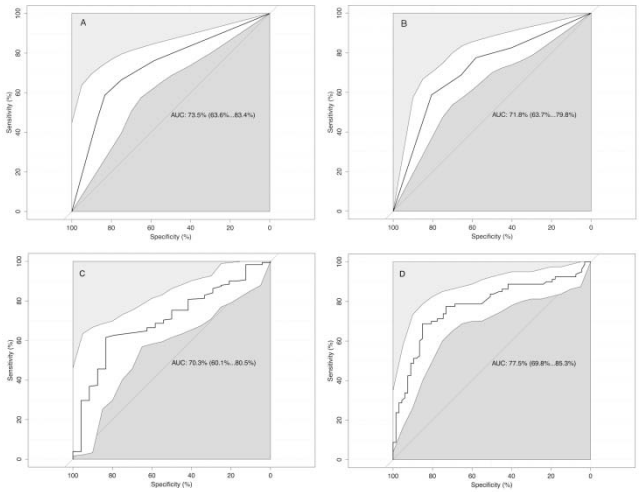

FIGURE 3. ROC analyses curves and 95% confidence intervals (white area) of the semi-quantitative scoring system (A) and TBR (B) for detection of any grade PCa and semi-quantitative scoring system (C) and TBR (D) for detection of GS ≥ 7 (3+4).

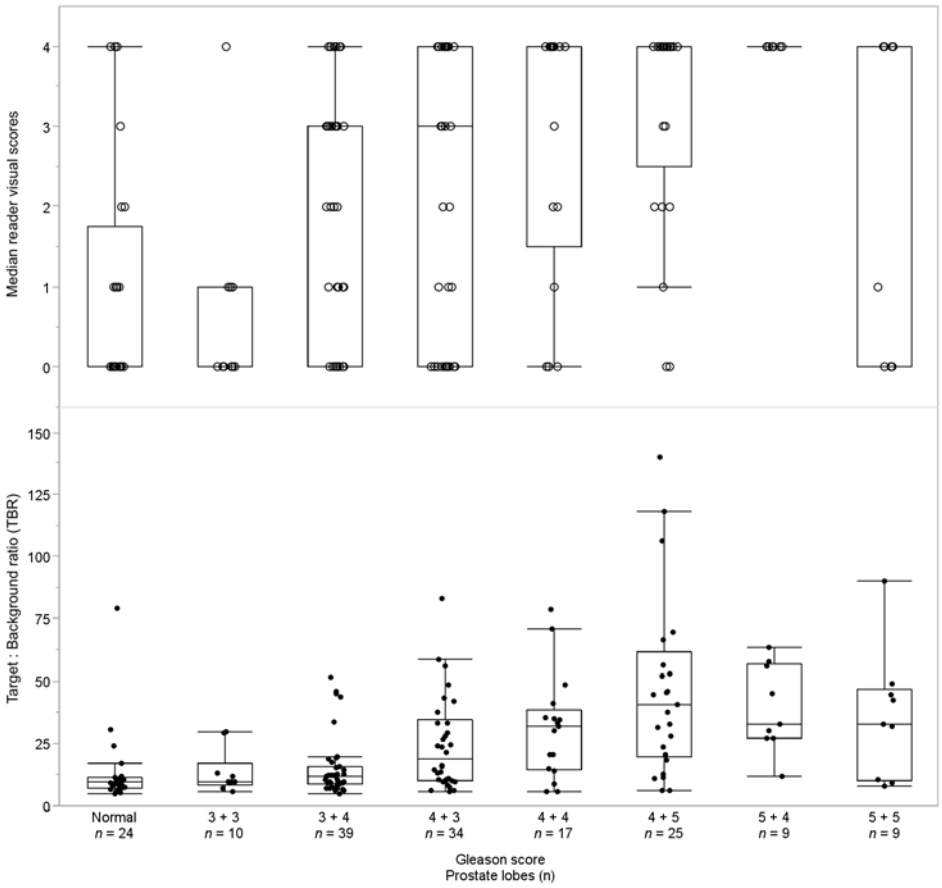

FIGURE 4. Box-and-whisker plots of mean reader scores (top row, open circles) and TBR values (bottom row, solid circles) in lobes with no PCa and in lobes with PCa of increasing GS.

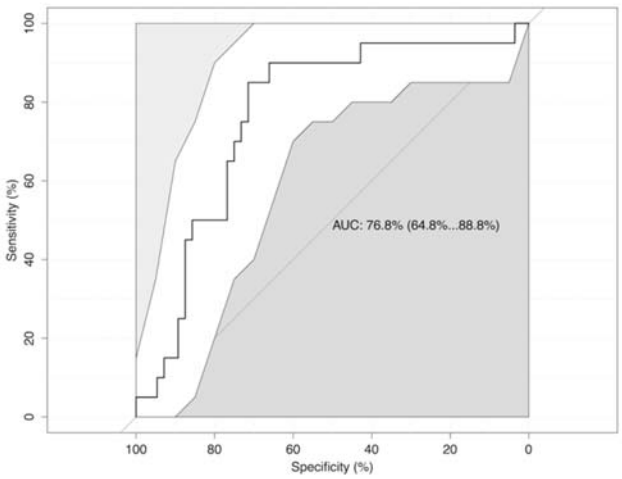

FIGURE 5. ROC analysis curves and 95% confidence intervals (white area) of TBR of the prostate lesion using a TBR cutoff of 30.2 to predict the presence of LNI. The maximal AUC is 0.77, yielding a sensitivity of 90% and a specificity of 67%.

TABLES

Table 1. Baseline characteristics of study population

Mean age (range)		63.2 years (46-77 years)
Clinical T-stage	T1c	1 (1%)
	T2	2 (1.9%)
	T2a	7 (6.7%)
	T2b	32 (30.5%)
	T2c	20 (19%)
	T3	4 (3.8%)
	T3a	29 (27.6%)
	T3b	10 (9.5%)
Race	White	102 (97%)
	Black	2 (1.9%)
	Asian	1 (1%)
Mean PSA (range)		27.0 ng/ml (2.4-372.7)
PSA	≤ 20	68 (65%)
	> 20	36 (35%)
Mean GS (range)		8 (6-9)
Biopsy GS	≤ 6	5 (5%)
	7	41 (39%)
	≥ 8	59 (56%)
Enrollment patients	US	40 (38%)
	Europe	65 (63%)
Ongoing ADT		20

PSA prostate specific antigen; GS Gleason score; ADT androgen deprivation therapy

Supplemental Figure 1

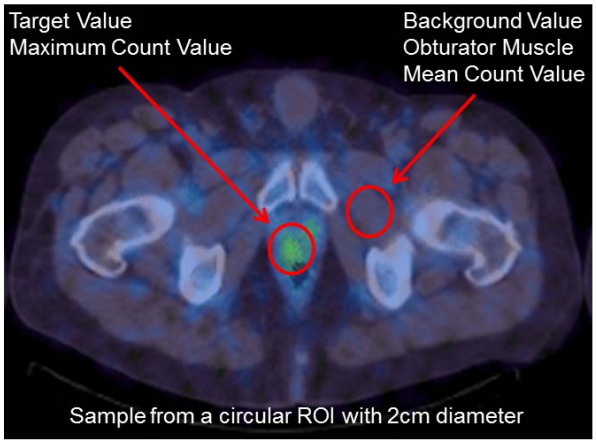

Supplemental Figure 1. Transverse slice of ^{99m}Tc-trofolastat SPECT/CT at the level of the prostate gland with representative circular ROIs over the lesion and within the obturator muscle.

Supplemental Table 1. Visual scoring scale

Score	Description	TBR
0	Equal to Background Activity/ No Contrast/No Lesions Observed	≤ 6
1	Slightly Above Background/Poor Contrast	> 6 and ≤ 8
2	Above Background/Good Contrast	> 8 and ≤ 10
3	Above Background/Excellent Contrast	> 10 and ≤ 15
4	Greater than all other activity/Excellent Contrast	> 15

TBR tumor-to-background ratio

Supplemental Table 2. Categorical mean uptake and visual scores

		TBR		*Visual scores*			
	N	*Mean*	*SD*	*Overall Median*	*Reader 1 Median*	*Reader 2 Median*	*Reader 3 Median*
SPECT scans*	103						
Treated	26	16.2	11.2	3.0	2.0	3.0	4.0
Untreated	77	37.7	35.6	4.0	3.0	4.0	4.0
Prostate Lobes*	206						
Treated	56	15.4	11.4	2.0	0.0	1.0	3.0
Untreated	150	28.1	30.6	3.0	2.0	1.0	4.0
Normal Lobes	24	13.5	15.2	0.0	0.0	0.0	2.5
Abnormal Lobes†	182	26.1	28.2	3.0	2.0	2.0	4.0
GS 6	12	12.3	8.3	0.5	0.0	0.5	3.0
GS 7	71	22.0	25.6	3.0	2.0	1.0	4.0
GS 8-10	60	41.3	34.6	4.0	3.0	4.0	4.0
GS ≤3+3	36	13.1	13.2	1.0	0.0	0.0	3.0
GS ≥3+4	131	30.8	31.4	4.0	3.0	3.0	4.0
Lymph node involvement††							
Yes	33	40.9	36.1	4.0	3.0	4.0	4.0
No	69	28.5	30.5	3.0	3.0	3.0	4.0

* 2 Patients had non-evaluable or missing SPECT/CT scans and/or pathology results (600-001, 801-001)
† 39 Prostate lobes were unevaluable for Gleason grade but noted as having histopathology consistent with PCa
†† 3 Patients had non-evaluable or missing lymph node pathology and/or missing or unevaluable SPECT/CT scans (101-002, 105-002, 600-001)

TBR target-to-background ratio, SD standard deviation, GS Gleason score

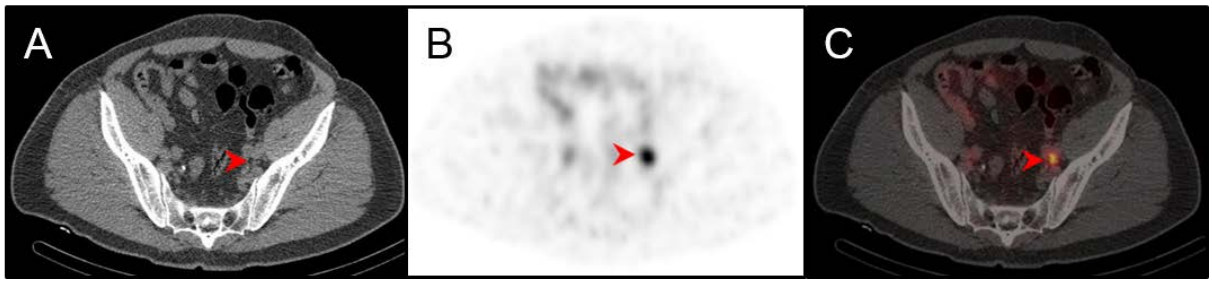

Supplemental Figure 2. Example of fused axial 99mTc-trofolastat SPECT/CT (C) with corresponding CT (A) and SPECT (B) slices showing a positive small lymph node in the left obturator fossa. Red arrow heads indicate location of histologically confirmed metastatic lymph node.